Three-Dimensional Structure Analysis of μ-Agatoxins: Further Evidence for Common Motifs among Neurotoxins with Diverse Ion Channel Specificities†

Diana O. Omecinsky,‡ Katherine E. Holub,‡ Michael E. Adams,§ and Michael D. Reily*,‡

Department of Chemistry, Parke-Davis Pharmaceutical Research Division of Warner Lambert Company, 2800 Plymouth Road, Ann Arbor, Michigan 48105, and Departments of Entomology and Neuroscience, University of California, Riverside, California 92521

Received November 2, 1995; Revised Manuscript Received December 12, 1995⊗

ABSTRACT: We report the solution structure of μ-agatoxin-I (μ-Aga-I) and model structures of the closely related μ-agatoxin-IV (μ-Aga-IV) which were isolated from venom of the American funnel web spider, *Agelenopsis aperta*. These toxins, which modify the kinetics of neuronal voltage-activated sodium channels in insects, are C-terminally amidated peptides composed of 36 amino acids, including four internal disulfide bonds. The structure of μ-Aga-I was determined by NMR and distance geometry/molecular dynamics calculations. Structural calculations were carried out using 256 interresidue NOE-derived distance restraints and 25 angle restraints obtained from vicinal coupling constants. The peptide contains eight cysteines involved in disulfide bonds, the pairings of which were uncertain and had to be determined from preliminary structure calculations. The toxin has an average rmsd of 0.89 Å for the backbone atoms among 38 converged conformers. The structure consists of a well-defined triple-stranded β-sheet involving residues 7−9, 20−24, and 30−34 and four tight turns. A homologous peptide, μ-Aga-IV, exhibited two distinct and equally populated conformations in solution, which complicated spectral analysis. Analysis of sequential NOE's confirmed that the conformers arose from cis and trans peptide bonds involving a proline at position 15. Models were developed for both conformers based on the μ-Aga-I structure. Our structural data show that the μ-agatoxins, although specific modifiers of sodium channels, share common secondary and tertiary structural motifs with phylogenetically diverse peptide toxins targeting a variety of channel types. The μ-agatoxins add voltage-sensitive sodium channel activity to a growing list of neurotoxic effects elicited by peptide toxins which share the same global fold yet differ in their animal origin and ion channel selectivity.

Spiders are one of many animal groups that use paralytic venoms for prey capture. A common feature among the peptide toxin components of these venoms is a highly constrained tertiary structure brought about by internal disulfide bonding. Recently, it has been pointed out that the ω-agatoxins and ω-conotoxins from spider and cone snail venoms, respectively, share common tertiary structure and cystine motifs despite their dissimilar primary structure and calcium channel specificities (Pallaghy et al., 1994; Narasimhan et al., 1994). These findings indicate that the core structures of these toxins are dictated more by their disulfide-bonding patterns than by their amino acid sequences.

The μ-agatoxins (Adams et al., 1989a; Skinner et al., 1989) are peptides from *Agelenopsis aperta* spider venom which produce excitatory paralysis in insects. Electrophysiological studies show that these toxins produce repetitive action potentials and alter neurotransmitter release from motor nerve terminals by modification of neuronal sodium channel properties, presumably by shifting the channel activation curve to more negative potentials (Adams et al., 1989a,b). Such actions are similar to the effects of various scorpion toxins on insect and mammalian neuronal sodium channels (Zlotkin et al., 1994).

Here we report the three-dimensional solution structure of μ-agatoxin-I (μ-Aga-I) obtained by NMR and distance geometry/molecular dynamics calculations. On the basis of this experimentally determined structure, we also propose models for two conformations of μ-Aga-IV, a highly homologous peptide with similar functional activity. Of particular interest are the structural features that the μ-agatoxins share with other toxins whose structures have been reported but which have altogether different animal origins and/or ion channel selectivities. These include peptides selective for P-type calcium channels (Reily et al., 1994, 1995; Mintz et al., 1992; Yu et al., 1993; Kim et al., 1995) and N-type calcium channels (Davis et al., 1993; Sevilla et al., 1993; Pallaghy et al., 1993; Basus et al., 1995) as well as various scorpion toxins that modify sodium channels (Zhao et al., 1992; Housset et al., 1994) and potassium channels (Johnson & Sugg, 1992; Bontems et al., 1991; Arseniev et al., 1984).

MATERIALS AND METHODS

NMR Spectroscopy. The μ-agatoxins were purified from crude *A. aperta* venom using chromatographic protocols described elsewhere (Adams et al., 1989a; Skinner et al., 1989). Samples for NMR contained 2−4 mg of peptide dissolved in 500 μL of either 99.96% D_2O or 90% H_2O/10% D_2O at pH 2.6.

All NMR spectra were collected on Bruker AMX500 and AMX600 spectrometers. A DQF-COSY[1] spectrum (Rance et al., 1983) was acquired at 298 K. TOCSY spectra (Braunschweiler & Ernst, 1983) with a 60 ms 7 kHz mlev-

† This work was supported in part by U.S. Public Health Service Grant NS24472 (to M.E.A.).

* Corresponding author.

‡ Parke-Davis Pharmaceutical Research Division of Warner Lambert Co.

§ University of California.

⊗ Abstract published in *Advance ACS Abstracts,* February 1, 1996.

0006-2960/96/0435-2836$12.00/0

16 (Bax & Davis, 1985) spin-lock field were acquired at 298, 303, and 308 K. NOESY spectra were acquired at 298 and 308 K with a 250 ms mixing time and at 303 K with 80, 120, and 250 ms mixing times. NOESY spectra in which the aliphatic protons were decoupled from cross relaxation with amide protons were recorded using the BD-NOESY pulse sequence (Macura et al., 1992; Hoogstraten et al., 1993). Decoupling during the 260 ms mixing sequence was accomplished using a continuous train of 5.0 ms (180°) hyperbolic secant pulses separated by 3 μs delays. The shaped pulses were digitally generated using Bruker software with a phase factor of 9 and a truncation level of 20% with 1024 points. Slowly exchanging amide protons were determined by dissolving the sample in 500 μL of D_2O at 298 K followed by collection of sequential 2D spectra to unambiguously assign the nonexchanged protons. Protons were classified as either slowly or very slowly exchanging on the basis of the presence of signals in simultaneously acquired NOESY ($t_{1/2}$ > 2 h) and DQF-COSY spectra ($t_{1/2}$ > 10 h), respectively. All NMR spectra were processed using UXNMR (Bruker Instruments). The real portions of the processed data were transferred to a Silicon Graphics workstation and converted to a Felix matrix format using the ux2mat program (P. Schmeider, personal communication). For 2D spectra, 1024 or 2048 complex points were acquired in the t_2 dimension and 512 or 700 points in t_1. The data were zero filled to a final matrix size of 2048 × 1024 or 4096 × 1024 points. Signal to noise was enhanced and truncation artifacts were minimized by application of a $\cos^2$ function in both dimensions prior to Fourier transformation. One-dimensional spectra contained 16K complex points. Quadrature detection in the t_1 dimension was achieved by the TPPI method in 2D spectra. Coupling constants were measured directly from resolution-enhanced 1D spectra recorded in H_2O.

For μ-Aga-IV, the TOCSY spectra were acquired at 290, 300, and 310 K. NOESY spectra were collected at 290 K with a mixing time of 400 ms and at 300 K with 150, 250, and 400 ms mixing times. The DQF-COSY was collected at 300 K.

Structure Determination. Distance restraints were calculated from NOESY cross-peak volumes using FELIX (Biosym Technologies) to both integrate well resolved cross-peaks and assign an upper bound distance based on measured volumes. The volume integrals obtained from the 250 ms NOESY spectrum were converted to upper bound distance restraints of 2.5, 3.5, or 5.5 Å corresponding to strong, medium, and weak NOE's, respectively. Intra-side-chain NOE's in Trp were used as scalar pairs for calibration of calculated upper bound restraints. In all cases the lower bounds were taken to be the sum of the van der Waals radii. When warranted, backbone ϕ angles were constrained to ranges consistent with measured $^3J_{HNH\alpha}$, and $\chi1$ angles for several amino acids were constrained on the basis of the relative magnitude of intraresidue Hα−Hβ and HN−Hβ NOEs and $^3J_{H\alpha,H\beta}$ (Wagner et al., 1987). Peptide bond planarity was ensured by inclusion of constraints for the ω torsion. Redundant torsion constraints for ω and ϕ were generated with the program CORTOR.[2]

Distance geometry calculations were performed using the distance geometry/simulated annealing program, DGII, and a subset of constraints including only NOE upper bound, ω torsion, and ϕ torsion restraints. Structures were generated using triangle bounds smoothing, a four-dimensional embed algorithm, and a simulated annealing stage with the initial energy set to 1024 kcal/mol. The final error threshold was set to 0.1 to ensure that none of the structures were minimized. Typically, final DGII errors of 0.2−0.5 were observed in successful structures whereas the corresponding mirror images gave errors about 10 times higher. This resulted in a set of DGII-derived structures that contained the correct stereochemistry and were properly folded. The constraints were removed, and optimized DGII structures were energy minimized with 100 steps of steepest descents, followed by 500 steps of conjugate gradient minimization. Full constraints, including chirality, $\chi1$, and hydrogen bond constraints, were then reapplied, and each molecule was subjected to another 500 steps of conjugate gradient minimization followed by molecular dynamics for 5 ps at 300 K during which time the force constant on the NOE constraints was gradually reduced from 40 to 30 kcal/mol. During this same period, dihedral force constants were increased from 80 to 160 kcal/mol. Finally, each member of the ensemble was energy minimized for 1000 steps (conjugate gradients) followed by 100 steps (steepest descents) with the constraints in place and using final force constants of 30 and 160 kcal/mol for distance and dihedral constraints, respectively. All calculations were performed in vacuo with charges turned off using the cvff91 force field (Biosym Technologies). This protocol resulted in structures that were lower in energy yet still had acceptable levels of violations from experimental constraints than the procedure previously described for ω-Aga-IVB (Reily et al., 1995). The precision of the final structures was evaluated using methods described previously (Hyberts et al., 1992).

Due to the presence of two isomers (see below) and the resulting complexity of the spectra for μ-Aga-IV, NOE cross-peaks were evaluated for only a limited number of unambiguously assigned long-range cross-peaks in the NOESY spectra (31 and 33 for the *cis*- and *trans*-Pro15 isomers, respectively). These cross-peaks were classified as strong, medium, and weak on the basis of their relative intensity, and corresponding internuclear upper bounds of 2.5, 3.5, and 5.0 Å were assigned and lower bounds were set as described above. A crude model of μ-Aga-IV was constructed using the coordinates of the lowest energy μ-Aga-I structure and inserting a His residue between position E15 and C16 and replacing the appropriate amino acid side chains. This crude model was then minimized using a conjugate gradient algorithm for 500 steps followed by a steepest descents algorithm for 100 steps with the P15 ω torsion constrained to 180° and the coordinates of the core residues fixed to produce a "*trans*-P15" model. The P15 ω torsion was then

[1] Abbreviations: TOCSY, total correlated spectroscopy; NOESY, nuclear Overhauser spectroscopy; BD-NOESY, block-decoupled nuclear Overhauser spectroscopy; DQF-COSY, double-quantum-filtered correlated spectroscopy; TPPI, time-proportional phase incrementation; $<\text{rmsd}>_{xy}$, root-mean-squared deviation from average coordinates, where *x* and *y* are the measured residues and atoms (backbone, bb, or heavy, hv), respectively.

[2] CORTOR is a program that generates redundant torsion constraints from single constraints for ϕ and ω torsion angles and was the kind gift of Frank Soennichsen and Robert Boyko at the Protein Engineering Network Centre of Excellence, University of Alberta, Edmonton, Canada T6G 2S2.

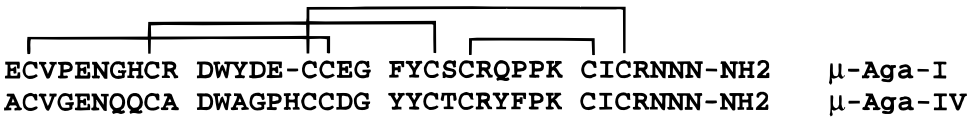

FIGURE 1: Sequences and disulfide-bonding pattern in μ-Aga-I and μ-Aga-IV.

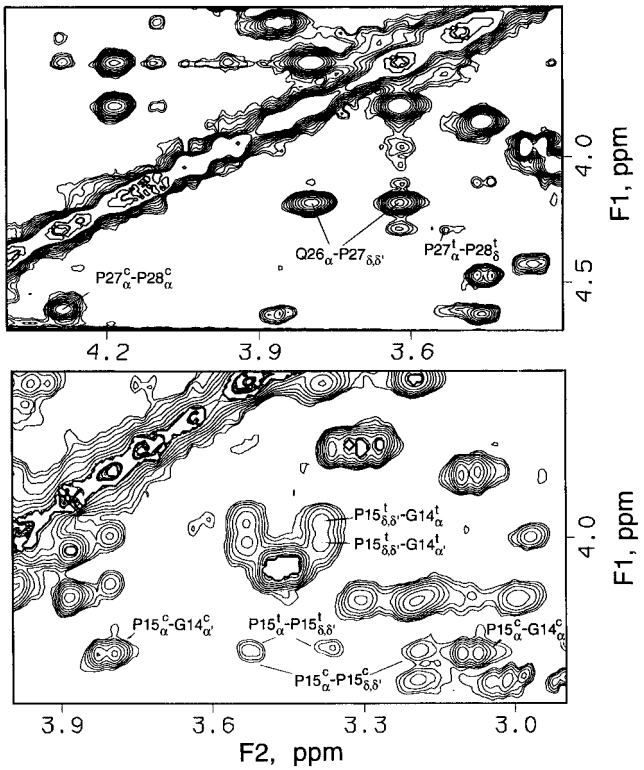

FIGURE 2: Selected regions of the NOESY spectrum recorded in D_2O showing cross-peaks critical for assignment of *cis*- and *trans*-proline configurations. Top: μ-Aga-I, 250 ms mixing time. Bottom: μ-Aga-IV, 400 ms mixing time. Selected assignments are indicated. Superscripts t and c refer to the *trans*- and *cis*-proline isomers, respectively.

constrained to 0°, and the same minimization procedure was followed to produce a "*cis*-P15" model. These cis and trans conformational models were then further minimized with the NOE constraints to obtain final μ-Aga-IV models.

RESULTS

NMR Spectral Analysis. The assignment of the NMR spectra was based on the spin system identification and sequential assignment techniques developed by Wüthrich and co-workers (Wüthrich, 1986). Under the conditions used in this study, μ-Aga-I exists predominantly as one isomer which contains a cis peptide bond between P27 and P28, as evidenced by an intense NOE between the α protons of these two residues. A minor conformer (~5%) was shown to be the trans proline isomer on the basis of a P27 Hα−P28 Hδ NOE. The NOE's that allowed us to establish the peptide bond configurations are shown in Figure 2A.

Analysis of the μ-Aga-IV spectra revealed two sets of signals of approximately equal intensity that complicated spectral analysis. Despite the duplicity of peaks, it was possible to confirm that cis/trans isomerization involving P15 was responsible for the spectral heterogeneity (Figure 2B). A strong cross-peak between F28 Hα and P29 Hα gives evidence that the *cis*-proline peptide bond seen between P27 and P28 in μ-Aga-I is conserved in both conformers of μ-Aga-IV (not shown). The relative intensity of the two conformers was not affected by temperature in the range of 27−37 °C. The resonance assignments for μ-Aga-I are provided in the supporting information.

Distance and Dihedral Angle Restraints. Fifteen ϕ angle restraints were determined from $^3J_{HNH\alpha}$ measured between 25 and 35 °C. Backbone ϕ angles were constrained to a range of −90° to −10° for residues 5, 11, 15, 17, 29, and 34 and −175° to −75° for residues 9, 20, 21, 23, 24, 26, 30, 31, and 33 on the basis of the measured $^3J_{HNH\alpha}$ (Clore et al., 1991). The ϕ angle for Asn6 was constrained between 10° and 90° on the basis of the $^3J_{HNH\alpha}$ of 7.0 Hz and the intense NH−Hα NOE observed (Ludvigsen & Poulsen, 1992). Stereospecific assignments and χ1 angle constraints were determined for eight residues, S23, C30, C22, R33 (160° to −160°), C17, C32, R33 (−80° to −40°), and C9 (40° to 80°), on the basis of the relative size of the two $^3J_{H\alpha,H\beta}$ coupling constants and the relative magnitude of the Hα−Hβ NOEs and NH−Hβ NOEs (Wagner et al., 1987). In addition, χ1 for C2 and C16 was constrained between 160° and −40° on the basis of the observation that $^3J_{H\alpha,H\beta2} \neq {}^3J_{H\alpha,H\beta3}$.

Possible acceptors for hydrogen bonds with the slowly and very slowly exchanging NH's were initially identified by searching within a 4 Å radius of each amide proton in the 50 DGII structures (which were generated without any constraints for hydrogen bonds). When unique acceptors were identified, a single upper bound distance restraint of 2.35 Å was used between the amide proton and the acceptor atom. In this way, hydrogen bonds were identified for all seven of the very slowly exchanging amino protons at positions 3, 17, 20, 21, 31, 32, and 33 and for five of the nine slowly exchanging residues 6, 7, 9, 23, and 29.

Disulfide Determination. The disulfide-bonding pattern for μ-Aga-I was inferred from the degradation analysis of the closely related μ-Aga-V (Skinner et al., 1989). In that report, peptide mapping determined two possible cysteine pairings: 2−17 and 16−32 or 2−16 and 17−32. One method of determining correct disulfide-bonding patterns relies on the observation of NOE's between protons of cysteine residues (Klaus et al., 1993). Disulfide bonds between C24−C30 and C2−C17 were indicated by the following NOE's: C24Hβ−C30Hα (medium intensity), C24Hα−C30Hα (medium intensity), C24Hβ−C30Hβ (weak intensity), C24Hα−C30Hβ (medium intensity), and C2Hβ−C17Hα (strong intensity). As a second method to assess the proper disulfides, we generated structures using the DG/MD protocol with starting structures constructed with alternative cysteine pairs. This method proved less useful, however, as the errors and final energies for both sets of structures were very similar. A third method was used where the starting structure had no disulfide bonds defined and the pairings of the cysteine residues were determined from statistical analyses of the cystine Cβ−Cβ interatomic distances in structures calculated using DGII. These results favored the C2−C17 pair, consistent with the observed

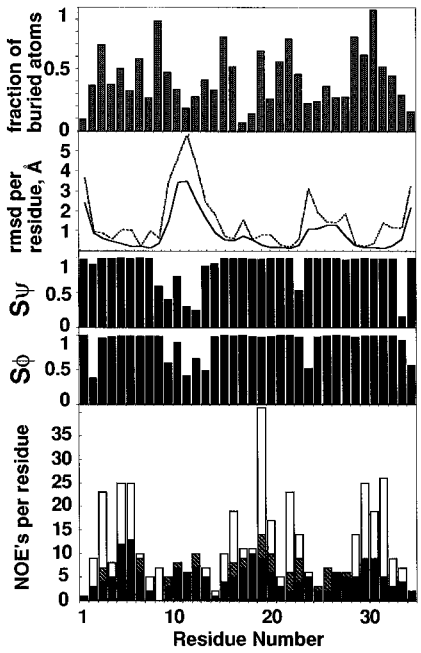

FIGURE 3: Summary of NOE constraints and structural parameters in μ-Aga-I. Bottom: Number of NOE constraints per residue. Solid, shaded, and open bars indicate sequential, medium, and long-range (>i−i+4) NOE's, respectively. Middle: Angular order parameters for backbone angles ψ, Sψ and ϕ, Sϕ, and Cartesian coordinate rmsd from the average for backbone atoms (solid line) and all heavy atoms (dotted line) for the 38 final structures. Top: Solvent-inaccessible residues in μ-Aga-I. The height of the bar indicates the fraction of atoms per residue that do not contact a 1.4 Å spherical probe in Connolly calculations on nine of the final structures (see text).

intercysteine NOE's, convincing us that the correct pairing for the ambiguous cysteines was C2−C17 and C16−32. The NMR data together with the previously reported proteolytic fragmentation results support the disulfide pattern shown in Figure 1. This disulfide pattern is identical to that of the ω-agatoxins (Nishio et al., 1993; Adams et al., 1993; Yu et al., 1993). The appropriate covalent disulfide bonds were incorporated into a randomly selected structure from the calculations performed without disulfide bond constraints. The energy of the resulting structure was minimized and used as a starting structure for subsequent calculations.

Structure Determination. After several iterations of structure calculation and data correction, a restraint set containing 256 interresidue upper bound restraints from NOE's (see Figure 3), 12 hydrogen bonds, 10 χ1, and 15 ϕ restraints was constructed. From this, 50 final structures were generated, of which 38 had no dihedral angle violations >5° and no distance violations >0.5 Å, and were used in subsequent discussion. Models for the two forms of μ-Aga-IV were prepared from the lowest energy structure of μ-Aga-I as described above.

DISCUSSION

Evaluation of the μ-Aga-I Structures. Figure 4 shows the final 38 converged structures superimposed by the backbone atoms of residues in the β-sheet region (see below). The final structures show variable <rmsd> values with a baseline around 0.3 Å and four regions of high <rmsd> and low order parameters corresponding to two loops and the C- and N-termini (Figure 3). The occurrence of high <rmsd> corresponds to regions for which we observed few long-range NOEs (Figure 3). Twenty-four of the 36 residues have S_ϕ and $S_\psi \geq 0.9$, most of which occur within the β region of the Ramachandran map (Figure 5). The only exceptions are P28, N6, and G19. P28 is the i+2 residue of a type VI turn, and the latter two are i+2 residues of type II β-turns; see below.

β-Sheet. During the resonance assignment stage, long-range backbone−backbone NOE's indicated the presence of a three-stranded antiparallel β-sheet comprised of residues 7−9, 20−24, and 30−34 (Figure 6). This β-sheet has the same +2x, −1 topology as other peptide toxins with this cystine motif, such as ω-Aga-IVA (Reily et al., 1994) and ω-Aga-IVB (Adams et al., 1993; Yu et al., 1993; Reily et al., 1995), and ω-conotoxin GVIA (Davis et al., 1993; Sevilla et al., 1993; Pallaghy et al., 1993). The β-sheet is well-defined, having an average <rmsd> of 0.23 and 0.63 Å for the backbone and heavy atoms, respectively. As was observed for ω-Aga-IVB (Adams et al., 1993; Reily et al., 1995), the coupling constants measured for some of these residues are smaller than expected for canonical ϕ angles found in β-sheets, suggesting an irregular sheet structure for some residues. The comparison to ω-Aga-IVB is discussed in further detail below.

Turns. Several turns in the peptide were initially identified by the standard criteria that Cαi is less than 7 Å from Cαi+3 and that the residues at i+1 and i+2 are not helical (Lewis et al., 1973). Analysis of the ensemble of final structures resulted in 4 i−i+3 pairs that were <7.0 Å apart in all of the 38 final structures: 4−7, 17−20, 24−27, and 26−29. Additionally, i−i+3 pairs were <7.0 Å apart between residues 10−13, 11−14, 12−15, and 27−30 in 35, 16, 14, and 35 of the final structures, respectively. Inspection of the ensemble allowed us to place these Cαi,Cαi+3 pairs into four strand-reversing loops, of which the first and third are well defined and the second and fourth appear to be more disordered (Figures 3 and 4). In addition to measuring the ϕ, ψ torsion angles for amino acids implicated in turns by the above analysis, classification of turns was corroborated by comparison of observed NOE's with expected distances in canonical turn types (Table 1).

The residues that comprise the first turn (loop I), P4−E5−N6−G7, are well-defined ($<\text{rmsd}>_{4-7bb}$ = 0.33 Å) (Figure 3). The average ϕ, ψ angles for E5 and N6 are −64°, 147° and 56°, 10°, respectively, classifying the turn as a $\beta\gamma$ type using Ramachandran nomenclature (Wilmot & Thornton, 1990) which is equivalent to a distorted type II β-turn. A strong NOE was observed between Hα_{i+1} and NH$_{i+2}$ but no NOE was observed between NH$_{i+1}$ and NH$_{i+2}$ in the BD-NOESY (Table 1), suggesting little or no contribution from $\alpha\alpha$ (type I) β-turn (Wüthrich, et al., 1983). Finally, G7 NH exchanges very slowly and is involved in a hydrogen bond to the P4 carbonyl oxygen (see below).

Loop II occurs between residues 10 and 15 and is difficult to evaluate because of the poor alignment of the structures and small angular order parameters. There are also multiple overlapping Cαi,Cαi+3 pairs for some structures in this region (see above). It is noteworthy to observe that there is a Trp in this region of the molecule that is conserved among the ω- and μ-agatoxins, and occupies the i+1 position in a $\beta\gamma$-type turn in ω-Aga-IVB (Reily et al., 1995). The average ϕ, ψ angles for D11 and W12 are −73°, 75° and 103°, −10°, respectively, indicating that, on average, the correct geometry for a $\beta\gamma$-type turn exists. However, these residues are poorly

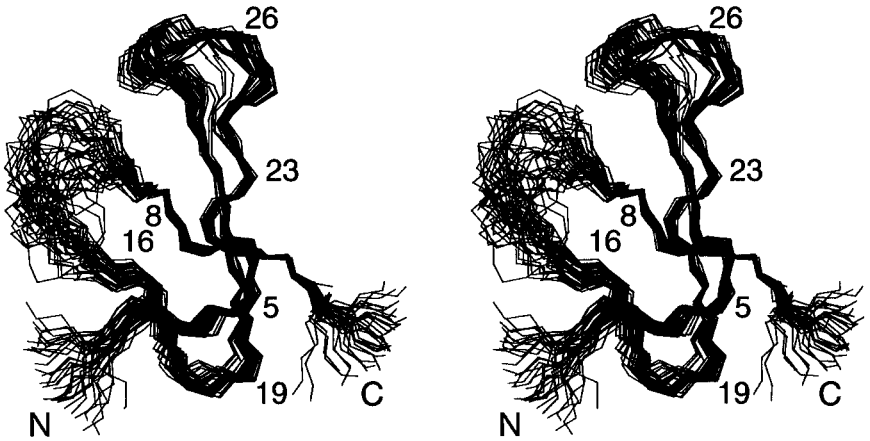

FIGURE 4: Defocused stereoviews of the backbone traces of 38 converged structures compared by superimposing backbone atoms in the β-sheet residues.

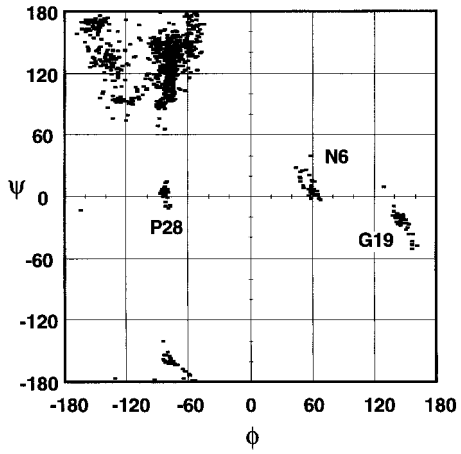

FIGURE 5: Ramachandran diagram for the 24 residues for which the ϕ and ψ order parameters are $\geq$0.9 in the 38 final structures. Residues lying outside the β region are labeled.

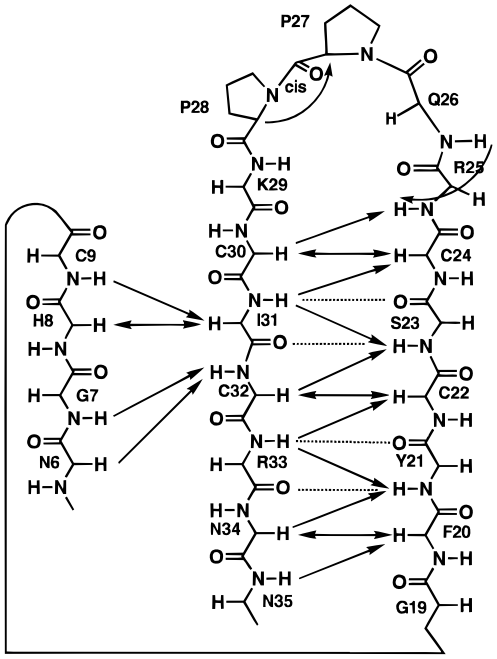

FIGURE 6: β-sheet structure in μ-Aga-I. Solid arrows indicate observed NOE's, and dotted lines indicate inferred hydrogen bonds.

ordered (<rmsd>$_{10-14bb}$ = 2.51 Å) due to a lack of NOE and coupling constant data in this region (Figure 3), and interpretation of the average angles may not be valid. The lack of experimental data in this region is due, in part, to moderately fast internal motion evidenced by unusually broad lines (>20 Hz at 25 °C) for the amide protons of the i+2 (W12) and i+3 (Y13) residues. The weak NH−NH NOE observed between D11 and W12 suggests that there is possibly some αα (type I) character in this turn (Table 1) and that interconversion between multiple turn types could be responsible for this line broadening. Only R10 has a slowly exchanging backbone amide proton, suggesting that the backbone amide protons of the amino acids in this loop do not participate in stable hydrogen bonding. The apparent disorder in this region of the molecule suggested by the line broadening and low precision in the ensemble of structures (Figure 3) precludes classification of this region into a single turn type.

Table 1: Selected Interproton Distances in Classical Turn Types and Relative NOE Intensities Utilized in Characterizing Turns in μ-Aga-I[a]

turn type/loop no.	$d\alpha_{i+1},N_{i+2}$	$d\ N_{i+1},N_{i+2}$	$d\alpha_{i+2},N_{i+3}$	$d\alpha_{i+1},N_{i+3}$
αα (I)	3.47	2.59	3.22	3.58
$\beta\gamma$ (II)	2.01	4.56	3.22	3.21
$\alpha\beta$ (VIII)	3.47	2.59	2.01	5.72
$\alpha\beta^{cisPro}$ (VIa)	4.60[b]	6.47[c]	3.36	2.70
$\beta\beta^{cisPro}$ (VIb)	4.69[b]	4.91[c]	2.14	2.96
loop I	S	no	S	*d*
loop II	S	W	M	M
loop III	S	no	S	S
loop IV, turn 1	M	S	S	no
loop IV, turn 2	W[b]	no[c]	M	S

[a] NH−NH NOE's were measured from a 260 ms BD-NOESY designed to eliminate aliphatic protons as pathways for spin diffusion (see text); all others were measured from a standard 250 ms phase-sensitive NOESY. no = no NOE was observed in a clear region of the NOESY spectrum above noise threshold at the expected cross-peak position. S, M, and W = strong, medium, and weak cross-peak intensity. [b] Closest $d\alpha_{i+1},\delta_{i+2}$ distance. [c] Closest $d\delta_{i+1},\delta_{i+2}$ distance. [d] Spectral overlap prevented measurement.

The third strand-reversing turn, loop III, is well ordered (<rmsd>$_{17-20bb}$ = 0.54 Å) and has average ϕ, ψ angles for E18 and G19 of −88°, 90° and 146°, −25°, respectively. This is consistent with observed NOE's (Table 1), and thus, as with loop I, this turn can also be classified as $\beta\gamma$ type.

The residues between the disulfide bond at 24 and 30 (loop IV) reverse the direction of the backbone between the two most prominent strands in the β-sheet. These residues have moderate deviations from the average structure, <rmsd>$_{26-29bb}$ = 1.11 Å. The relative position of the two strands of β-sheet

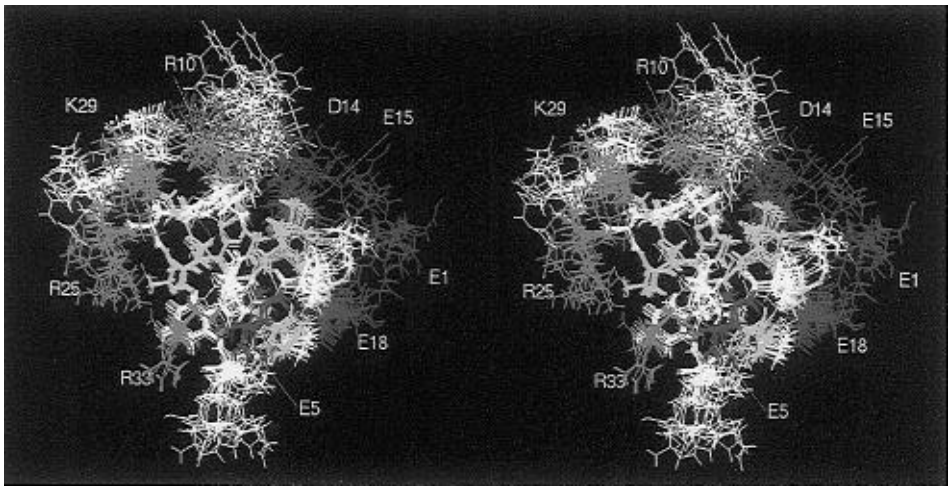

FIGURE 7: Defocused stereoviews of the charge distribution in the three-dimensional structure of μ-Aga-I. Shown are nine superimposed structures showing the location of the negatively (red) and positively (blue) charged side chains in μ-Aga-I. Amino acids which are largely unexposed to solvent (see text) are colored yellow. The set of atoms used for superposition and the backbone orientation are the same as in Figure 4.

is unambiguous on the basis of the large number of cross-strand NOE's observed (Figure 6). The characteristic NOE pattern for β-sheets largely disappears between cystines 24 and 30, suggesting that the interstrand disulfide bonds terminate the sheet and leave residues 25−29 to form the hairpin. This is similar to the case in ω-Aga-IVB, in which a strand−Cys−loop−Cys−strand motif makes up part of a β-sheet that ends abruptly at the interstrand disulfide pair and the two antiparallel strands are connected by a flexible loop (Reily et al., 1995). In the μ-agatoxins, the loop is one residue shorter than in ω-Aga-IVB. Loop IV is characterized by two close $i-i+3$ contacts in all of the structures (24−27 and 26−29), suggesting the presence of two sequential turns. Within the loop region, the N-terminal turn has average ϕ, ψ values of −54°, −56° and −125°, 95° for $i+1$ (R25) and $i+2$ (Q26), respectively, although R25 ϕ is disordered. This disorder is the result of well-defined major (29 structures) and minor (9 structures) conformational families with average ϕ angles of −69° and 79°, respectively. In the major family this turn adopts an $\alpha\beta$ (type VIII) configuration, while in the minor it exists in a $\gamma\beta$ configuration. The turn classification for the minor family does not correspond to a classical turn type, but there are at least eight examples of $\gamma\beta$-turns in the proteins (Wilmot & Thornton, 1990). The observed NOE's are consistent with an $\alpha\beta$-turn (Table 1), but the data do not rule out the possibility of multiple conformations in fast exchange.

The second (C-terminal) turn in loop IV is a β-turn involving residues 26−29, with a *trans*-proline at the $i+1$ position and a *cis*-proline at the $i+2$ position. Consistent with this is the K29 NH−Q26 O hydrogen bond observed in 34 of the 38 final structures. The type VI turn requires a *cis*-proline at position $i+2$ and can be further classified as $\alpha\beta^{\text{cisPro}}$ (type VIa) or $\beta\beta^{\text{cisPro}}$ (type VIb).[3] The average ϕ, ψ angles for P27 and P28 are −65°, 141° and −84°, 4°, consistent with an $\alpha\beta^{\text{cisPro}}$ turn. Experimental support for this assignment comes from the observation of a stronger NOE between $H\alpha_{i+1}$ and NH_{i+3} than between $H\alpha_{i+2}$ and NH_{i+3} (Table 1) (Dyson et al., 1988). This, together with the fact that a hydrogen bond is not normally observed in a $\beta\beta^{\text{cisPro}}$ turn (Richardson, 1988) argues for a $\alpha\beta^{\text{cisPro}}$ classification. In order to determine whether this particular sequence displayed any conformational preference in proteins, we conducted a survey of the Brookhaven Protein Data Bank and found 15 high-resolution protein structures containing a Pro-*cis*-Pro sequence. Of these, 13 (1CA2, 1CP4, 1HEA, 1HEB, 1HEC, 1HED, 2CA2, 2CAB, 2CPP, 3CA2, 3CPP, 6CPP, 7CPP) contained this sequence in an $\alpha\beta^{\text{cisPro}}$ turn and two (3RP2, 3RP2) in a $\beta\beta^{\text{cisPro}}$ turn.

Core Residues. As with other peptides that share this "cystine motif", the disulfide bonds constrain the cystine-rich region of μ-agatoxins in three-dimensional space (Narasimhan et al., 1994; Pallaghy et al., 1994). As expected for such a small protein, most of the residues are solvent-exposed. Residues that were partly buried and thus shielded from solvent were identified for the ten lowest energy structures as previously described (Reily et al., 1995). A majority of the solvent-shielded atoms arose from cysteines 9, 16, 17, 22, 30, and 32. In addition, parts of V3, G7, F20, S23, and I31 were close to the side chains of these cysteines and were substantially shielded from solvent (Figures 3 and 7). Each of the 11 residues identified in this way shows a large number of long- and medium-range NOE's (Figure 3). It is interesting to note that all of the solvent-shielded residues reported for ω-Aga-IVB correspond directly to solvent-shielded residues in μ-Aga-I, further evidence for the conservation of tertiary structure between these two functional classes.

Hydrogen Bonds. Sixteen of the 31 backbone amide protons were classified as slowly or very slowly exchanging, with several persisting even after 48 h. Amide protons that exchange slowly with deuterium from solvent must be shielded from solvent. The amide protons, thus removed from the electrostatic sink of bulk solvent, must satisfy their partial positive charge, and one mechanism for this is through hydrogen bonding. Good hydrogen bond geometry was observed for the following NH−O pairs in most of the final structures: 3−15, 6−32, 7−4, 9−30, 17−3, 20−17, 21−33, 23−31, 29−26, 31−23, 32−7, and 33−21. These pairs

[3] Some discrepancy exists regarding the type VI turn nomenclature as it relates to Ramachandran nomenclature. According to classical turn definitions (Richardson, 1981) a type VIb turn corresponds to a $\beta\beta^{\text{cisPro}}$ and not to an $\alpha_R\beta^{\text{cisPro}}$ as originally described (Wilmot & Thornton, 1990).

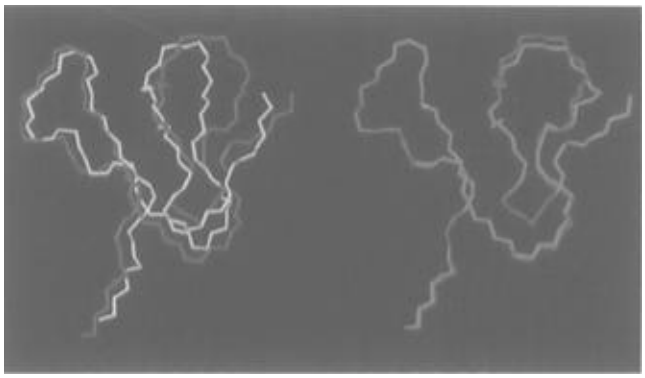

FIGURE 8: Modeled structures of μ-Aga-IV (backbone atom traces). Left: Superposition of the backbone atoms of the lowest-energy member of the μ-Aga-I ensemble (red) and the "*trans*-P15" model of μ-Aga-IV (yellow). Right: Superposition of the backbone atoms of the "*trans*-P15" (red) and "*cis*-P15" (green) models of μ-Aga-IV.

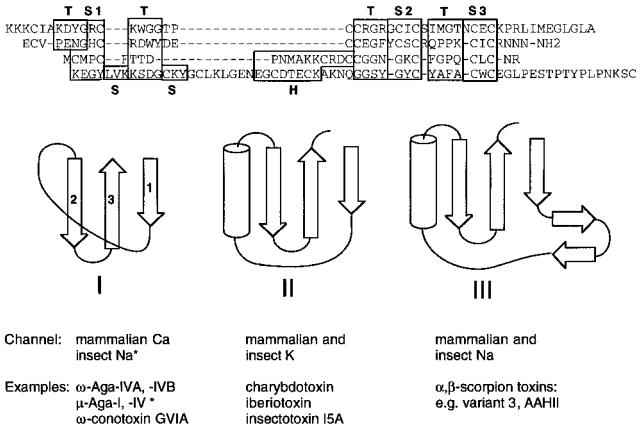

FIGURE 9: Comparison of primary and secondary structural elements in ion channel active peptides found in spiders, snails, and scorpions. The sequences (and their respective PDB entries) shown are (from top to bottom) ω-Aga-IVA (1IVA), μ-Aga-I (this work), insectotoxin I5A (1SIS), and scorpion neurotoxin variant 3 (2SN3). In the sequence alignment, secondary structural elements are designated as follows: S1−S3 = strands of the conserved β-sheet; S = strands from other β-sheets; T = turn; H = helix. See text for references to example toxins.

correspond to the simple H−O upper bound distance constraints used in the calculations and satisfy all of the very slowly exchanging and most of the slowly exchanging NH's.

Charged Residues. Like peptide toxins that specifically block voltage-sensitive calcium channels such as the ω-conotoxins and ω-agatoxins, the μ-agatoxins carry a large number of positively charged side chains. The two classes are dissimilar, however, in that the μ-agatoxins are neutral or anionic due to the presence of numerous acidic amino acids (the neutral ω-Aga-IVB is a notable exception). Within the μ-agatoxins, the location of charged side chains is well conserved, with the N- and C-termini carrying the bulk of the negative and positive charge, respectively. This charge distribution across the primary sequence is also observed in the closely related curtatoxins (Stapleton et al., 1990). The dipolar nature of the formal charge orientation in three dimensions is even more striking, with opposite charges on opposite sides of the molecule (Figure 7). It is intriguing to note that there are at least two reported cases of pairs of closely related peptides with identical biological targets, but which differ in their molecular dipole moments. One case is that of iberiotoxin and charybdotoxin in which a larger dipole moment in iberiotoxin is correlated with slower binding kinetics in maxi-potassium channels (Johnson & Sugg, 1992). A similar conclusion was reached in the case of ω-Aga-IVA and ω-Aga-IVB where the latter peptide and a chimera of the two have a larger dipole moment and slower kinetics of block and unblock of Ca^{2+} flux in rat Purkinje cells (Reily et al., 1994; Adams et al., 1993). The slight variations in charge distribution among the natural μ-agatoxins represent an excellent opportunity to further investigate this phenomenon.

μ-Aga-IV Model. The major differences in primary sequence between μ-Aga-I and μ-Aga-IV occur in the N-terminal half (Figure 1). Of these differences, perhaps the largest impact on three-dimensional structure might be expected to result from the Glu-to-Pro substitution at position 15 and the insertion of an additional amino acid (His) immediately following it. Models for the *trans*- and *cis*-P15 μ-Aga-IV show that the effect of the single His insertion at position 16 and the cis−trans isomerization of the G14−P15 bond have a pronounced impact on the backbone conformation (Figure 8). It is interesting to note that position 15 is at the C-terminal portion of the most disordered part of the μ-Aga-I structures (Figures 3 and 4). In μ-Aga-I, the amide protons of W12, Y13, and D14 are extremely broad while the corresponding NH's are sharper in both the cis and trans conformations of μ-Aga-IV. Thus, although the cis−trans isomerization of P15 results in two conformations of μ-Aga-IV, each of these may be more conformationally restricted in this particular region than the corresponding amino acids in μ-Aga-I. Overall, the conformational effect of the amino acid substitution and insertion in μ-Aga-IV is difficult to interpret given the high degree of disorder in this region of the ensemble of μ-Aga-I structures.

Comparison to Other Peptide Toxins. Recently, the three-dimensional structures of numerous peptides which specifically interact with different cellular ion channels have been reported. Emerging from these studies is the conclusion that peptide toxins found in venomous animals of different phyla contain similar structural motifs (Narasimhan et al., 1994; Pallaghy et al., 1994; Menez et al., 1992; Bontems et al., 1991). The work related here allows us to compare the μ-agatoxin structures with those of peptides found in diverse animals, including scorpions, spiders, and cone snails which act at other distinct ion channel targets. Among these are the well-characterized voltage-sensitive sodium channel and calcium-activated potassium channel antagonists found in species of scorpion and the ω-agatoxins and ω-conotoxins which act at P-type and N-type calcium channels, respectively [for reviews, see Adams and Swanson (1994), Olivera et al. (1994), and Adams and Olivera (1994)]. Despite the relative lack of sequence homology between these toxins and contrary to *a priori* expectations based on their evolutionarily divergent sources, these peptides share a common fold and can be grouped together on the basis of the central structural element of a three-stranded β-sheet with $2x, -1$ topology (Figure 9). The three structural subsets listed differ in the motif connecting strands 1 and 2. In the case of the ω-conotoxins and ω- and μ-agatoxins, this connecting motif is a short loop, whereas in the scorpion toxins, it is a loop−helix or a β-sheet−loop−helix motif.

Group I (Figure 9) includes calcium channel-active peptides from spider and cone snail venoms. Within this group there is a remarkable degree of similarity in backbone

conformation that is conveyed by a disulfide-bonding pattern and which transcends phylogenetic groups (Narasimhan et al., 1994; Pallaghy et al., 1994). The μ-agatoxins add voltage-sensitive sodium channel activity to this structural classification. Although there are no three-dimensional structures available, the disulfide-bonding pattern of recently reported δ-conotoxins (Fainzilber et al., 1994, 1995; Shon et al., 1994) suggests that they may constitute an additional family of sodium channel toxins falling into the group I motif.

The similarities in fold between various scorpion toxins that fall into structural groups II and III have been reported (Zhou et al., 1992). Group II includes the so-called "short" scorpion toxins, charybdotoxin (Bontems et al., 1991), iberiotoxin (Johnson & Sugg, 1992), and insectotoxin I5A (Arseniev et al., 1984). The scorpion toxins in this class that have been functionally characterized invariably modify potassium channels. Interestingly, other members of this class include the functionally unrelated defensins produced by insects (Bontems et al., 1991). Peptides within group II are similar in size and number of cysteine residues as those in group I, although a different disulfide spacing and bonding pattern stabilizes a helical segment between the first and last strand of the core β-sheet (Figure 9). Group III includes α- and β-scorpion toxins that bind to distinct sites on mammalian (Zhou et al., 1992; Catterall, 1986; Housset et al., 1994) and insect (Zlotkin et al., 1994; Fontecilla-Camps, J. C., 1989) sodium channels. At 60−70 residues, toxins in this group are considerably larger than those in groups I and II. All of the group III toxins have eight cysteines, and although different disulfide arrangements occur in different peptides, the overall fold is preserved in these large scorpion toxins (Fontecilla-Camps, 1989).

Even though structural complexity varies between groups, residues that are highly conserved within (and between) groups appear in all of the β-sheet strands (Figure 9). The conserved residues appearing in the core β-sheet include many of the cystines, which, although disulfide-bonding patterns vary between and within groups, are critical to maintenance of the three-dimensional structures. It has also been postulated and experimentally verified that specific side chains in the core β-sheet are also important for channel recognition (Zhao et al., 1992; Johnson & Sugg, 1992). Taken together, these points argue that the central three-stranded β-sheet is a common structural entity.

As a final note, the μ-agatoxins bear a close resemblance in primary structure to the curtatoxins isolated from the closely related spider *Hololena curta* (Stapleton et al., 1990). Although the interspecies peptide sequences are highly homologous, the limited biological data suggest that the activity of the curtatoxins may be different from the μ-agatoxins (flaccid vs excitatory paralysis). Despite the apparent differences in binding site and/or mode of action, one can reasonably conclude that the tertiary structures of the curtatoxins are likely to be quite similar to the μ-agatoxins.

CONCLUSIONS

In this paper, we have elucidated the three-dimensional structure of a μ-Aga-I and proposed models for the related μ-Aga-IV.[4] It is clear that the μ-agatoxins are members of a closely related structural class which includes peptides from spiders and cone snails that act as antagonists at mammalian calcium channels and whose principle structural component is a three-stranded β-sheet. It is interesting to note that the loop size and the core residues of the cystine-rich portion of μ-Aga-I and ω-Aga-IVB (and ω-Aga-IVA) are nearly identical and the main structural difference lies in the presence of a long, hydrophobic C-terminal tail in the latter peptide. In contrast, known N-type calcium channel-selective antagonists (e.g., ω-conotoxins) have both smaller cystine-constrained loops and lack a C-terminal tail. Thus, disregarding sequence and looking only at global fold, it appears that despite their functional diversity, the peptides from *Agelenopsis* are closer structurally to one another than are the more functionally related toxins from different animal classes. This is also apparent upon inspection of scorpion toxins. As has already been mentioned, the μ-agatoxins (and other members of group I) (Figure 9) are a structural subset of the more complicated scorpion toxins by virtue of the core β-sheet. Within the scorpion toxins, we find functional properties which are quite divergent (K vs Na channel activity, insect-selective vs mammal-selective), and yet these peptides have in common a three-stranded sheet with a helical linker between strands 1 and 2. If we limit our discussion to scorpion toxins that interact with sodium channels, all are 60−70 amino acids long and some are insect-active (e.g., LqhαIT) and, at least macroscopically, are functionally similar to the μ-agatoxins. It is curious that the scorpion has not instead evolved the simpler μ-agatoxin scaffold, since it could more efficiently accomplish the same goal, that is, to paralyze by interacting with voltage-sensitive sodium channels in its prey.

Interaction between peptide toxins and their ion channel targets is a complicated issue which is far from being completely understood. Our ability to study such interactions is hampered by the enormous size of target molecules which present multiple binding sites and thus far have been impossible to observe directly at atomic resolution. Despite the fact that the gross structure of ion channels is conserved between distant organisms, animal group specificity is common and has been noted in venoms or toxins from a variety of animals (Zlotkin et al., 1994). This latter point can be exploited in much the same way as studying the effect of toxin sequence on ion channel recognition. Powerful insights into the nature of toxin-channel interactions will be afforded by a knowledge of the three-dimensional structure of toxin molecules and the structure of channels from various animals.

ACKNOWLEDGMENT

Thanks to Mr. Chris Ingalls for writing the computer programs to calculate both the rmsd and order parameters and to analyze the hydrogen bonding. Thanks also to Dr. Venkataraman Thanabal for helpful discussions.

SUPPORTING INFORMATION AVAILABLE

One table containing proton resonance assignments and $^3J_{NHH\alpha}$ and NH exchange information for μ-Aga-I (1 page). Ordering information is given on any current masthead page.

[4] The coordinates for the ten lowest energy ω-Aga-I structures, along with models for the "cis-P15" and "trans-P15" models of μ-Aga-IV, are deposited in the Brookhaven Protein Data Bank. The ID codes for these entries are 1eit, 1eiu, and 1eiv, respectively.

REFERENCES

Adams, M. E., & Swanson, G. (1994) *Trends Neurosci.* (April 1994, Suppl.), 1−27.

Adams, M. E. (1994) in *Natural and Engineered Pest Management Agents* (Hedin, P. A., Menn, J. J., & Hollingworth, R. M., Eds.) pp 249−258, American Chemical Society, Washington, DC.

Adams, M. E., & Olivera, B. M. (1994) *Trends Neurosci. 17*, 151−155.

Adams, M. E., Herold, E. E., & Venema, V. J. (1989a) *J. Comp. Physiol. 164*, 333−342.

Adams, M. E., Bindokas, V. P., & Zlotkin, E. (1989b) *Insecticide Action. From Molecules to Organism* (Narahashi & Chambers, Eds.) pp 189−203, Plenum, New York, NY.

Adams, M. E., Mintz, I. M., Reily, M. D., Thanabal, V., & Bean, B. P. (1993) *Mol. Pharmacol. 44*, 681−688.

Arseniev, A. S., Kondakov, V. I., Maiorov, V. N., & Bystrov, V. F. (1984) *FEBS Lett. 165*, 57−62.

Basus, V. J., Nadasdi, L., Ramachandran, J., & Miljanich, G. P. (1995) *FEBS Lett. 370*, 163−169.

Bax, A., & Davis, D. G. (1985) *J. Magn. Reson. 65*, 355−360.

Bontems, F., Roumestand, C., Gilquin, B., Ménez, A., & Toma, F. (1991) *Science 524*, 1521−1523.

Braunschweiler, L., & Ernst, R. R. (1983) *J. Magn. Reson. 53*, 521−528.

Catterall, W. A. (1992) *Physiol. Rev. 72 (Suppl.)*, 515−548.

Clore, G. M., Wingfield, P. T., & Gronenborn, A. M. (1991) *Biochemistry 30*, 2315−2323.

Davis, J. H., Bradley, E. K., Miljanich, G., Nadasdi, L., Ramachandran, J., & Basus, V. (1993) *Biochemistry 32*, 7396−7405.

Dyson, J. H., Rance, M., Houghten, R. A., Lerner, R. A., & Wright, P. E. (1988) *J. Mol Biol. 201*, 161−200.

Fainzilber, M., Kofman, O. J., Zlotkin, E., & Gordon, D. (1994) *J. Biol. Chem. 269*, 2574−2580.

Fainzilber, M., Lodder, J. C., Kits, K. S., Kofman, O., Vinnitsky, I., Van Rietschoten, J., Zlotkin, E., & Gordon, D. (1995) *J. Biol. Chem. 270*, 1123−1129.

Fontecilla-Camps, J. C. (1989) *J. Mol. Evol. 29*, 63−67.

Goldstein, S. A. N., Pheasant, D. J., & Miller, C. (1994) *Neuron 12*, 1377−1388.

Hoogstraten, C. G., Westler, W. M., Macura, S., & Markley, J. L. (1993) *J. Magn. Reson. B 102*, 232−235.

Housset, D., Habersetzer-Rochat, C., Astier, J.-P., & Fontecilla-Camps, J. C. (1994) *J. Mol. Biol. 238*, 88−103.

Hyberts, S. G., Goldberg, M. S., Havel, T. F., & Wagner, G. (1992) *Protein Sci. 1*, 736−751.

Johnson, B. A., & Sugg, E. E. (1992) *Biochemistry 31*, 8151−8159.

Kim, J. I., Konishi, S., Iwai, H., Khono, T., Gouda, H., Shimada, I., Sato, K., & Arata, Y. (1995) *J. Mol. Biol. 250*, 659−671.

Klaus, W., Broger, C., Gerber, P., & Senn, H. (1993) *J. Mol. Biol. 232*, 897−906.

Kumar, A., Ernst, R. R., & Wüthrich, K. (1980) *Biochem. Biophys. Res. Commun. 95*, 1−6.

Lewis, P. N., Momany, F. A., & Scheraga, H. A. (1973) *Biochim. Biophys. Acta 303*, 211−229.

Ludvigsen, S., & Poulsen, F. M. (1992) *J. Biomol. NMR 2*, 227−233.

Macura, S., Fejzo, J., Hoogstraten, C. G., Westler, W. M., & Markley, J. L. (1992) *Isr. J. Chem. 32*, 245−256.

Marion, D., & Wüthrich, K. (1983) *Biochem. Biophys. Res. Commun. 113*, 967−974.

Ménez, A., Bontems, F., Roumestand, C., Gilquin, B., & Toma, F. (1992) *Proc. R. Soc. Edinburgh 99B*, 83−103.

Mintz, I. M., Venema, V. J., Swiderek, K. M., Lee, T. D., Bean, B. P., & Adams, M. E. (1992) *Nature (London) 355*, 827−829.

Narasimhan, L., Singh, J., Humblet, C., Guruprasad, K., & Blundell, T. (1994) *Nat. Struct. Biol. 1*, 850−852.

Nishio, H., Kumagaye, K. Y., Kubo, S., Chen, Y. N., Momiyama, A., Takahashi, T., Kimura, T., & Sakakibara, S. (1993) *Biochem. Biophys. Res. Commun. 196*, 1447−1453.

Olivera, B. M., Miljanich, G. P., Ramachandran, J., & Adams, M. E. (1994) *Annu. Rev. Biochem. 63*, 823−867.

Pallaghy, P. K., Duggan, B. M., Pennington, M. W., & Norton, R. S. (1993) *J. Mol. Biol. 234*, 405−420.

Pallaghy, P. K., Nielsen, K. J., Craik, D. J., & Norton, R. (1994) *Protein Sci. 3*, 1833−1836.

Rance, M., Sørenson, O. W., Bodenhausen, G., Wagner, G., Ernst, R. R., & Wüthrich, K. (1983) *Biochem. Biophys. Res. Commun. 117*, 479−485.

Reily, M. D., Holub, K. E., Gray, W. R., Norris, T. M., & Adams, M. E. (1994) *Nat. Struct. Biol. 1*, 853−856.

Reily, M. D., Thanabal, V., & Adams, M. E. (1995) *J. Biomol. NMR 5*, 122−132.

Richardson, J. S. (1981) *Adv. Protein Chem. 34*, 167−339.

Sevilla, P., Bruix, M., Santoro, J., Gago, F., Garcia, A. G., & Rico, M. (1993) *Biochem. Biophys. Res. Commun. 192*, 1238−1244.

Shon, K.-J., Hasson, A., Spira, M. E., Cruz, L. J., Gray, W. R., & Olivera, B. M. (1994) *Biochemistry 33*, 11420−11425.

Skinner, W. S., Adams, M. E., Quistad, G. B., Kataoka, H., Cesarin, B. J., Enderlin, F. E., & Schooley, D. A. (1989) *J. Biol. Chem. 264*, 2150−2155.

Stapleton, A., Blankenship, D. T., Ackermann, B. L., Chen, T. M., Gorder, G. W., Manley, G. D., Palfreyman, M. G., Coutant, J. E., & Cardin, A. D. (1990) *J. Biol. Chem. 265*, 2054−2059.

Valentino, K., Newcomb, R., Gadbois, T., Singh, T., Bowersox, S., Bitner, S., Justice, A., Yamashiro, D., Hoffman, B. B., Ciaranello, R., Miljanich, G., & Ramachandran, J. (1993) *Proc. Natl. Acad. Sci. U.S.A. 90*, 7894−7897.

Wagner, G., Braun, W., Havel, T. F., Schaumann, T., Gō, N., & Wüthrich, K. (1987) *J. Mol. Biol. 196*, 611−639.

Wilmot, C. M., & Thornton, J. M. (1990) *Protein Eng. 3*, 479−493.

Wüthrich, K. (1986) *NMR of Proteins and Nucleic Acids*, J. Wiley and Sons, New York.

Wüthrich, K., Billeter, M., & Braun, W. (1983) *J. Mol. Biol. 169*, 949−961.

Yu, H., Rosen, M. K., Saccomano, N. A., Phillips, D., Volkmann, R. A., & Schreiber, S. L. (1993) *Biochemistry 32*, 13123−13129.

Zhao, B., Carson, M., Ealick, S. E., & Bugg, C. E. (1992) *J. Mol. Biol. 227*, 239.

Zlotkin, E., Eitan, M., Pelhate, M., Chejanovsky, N., Gurevitz, M., & Gordon, D. (1994) *J. Toxicol., Toxin Rev. 13*, 25−43.

BI952605R